Biexciton recombination rates in self-assembled quantum dots

Michael Wimmer,[1,2,*] S. V. Nair,[3] and J. Shumway[2,†]
[1]*Institut für Theoretische Physik, Universität Regensburg, 93040 Regensburg, Germany*
[2]*Department of Physics and Astronomy, Arizona State University, Tempe, Arizona 85287-1504, USA*
[3]*Centre for Advanced Nanotechnology, University of Toronto, Toronto, Ontario, Canada M5S 3E3*
(Received 1 December 2005; published 7 April 2006)

The radiative recombination rates of interacting electron-hole pairs in a quantum dot are strongly affected by quantum correlations among electrons and holes in the dot. Recent measurements of the biexciton recombination rate in single self-assembled quantum dots have found values spanning from two times the single exciton recombination rate to values well below the exciton decay rate. In this paper, a Feynman path-integral formulation is developed to calculate recombination rates including thermal and many-body effects. Using real-space Monte Carlo integration, the path-integral expressions for realistic three-dimensional models of InGaAs/GaAs, CdSe/ZnSe, and InP/InGaP dots are evaluated, including anisotropic effective masses. Depending on size, radiative rates of typical dots lie in the regime between strong and intermediate confinement. The results compare favorably to recent experiments and calculations on related dot systems. Configuration interaction calculations using uncorrelated basis sets are found to be severely limited in calculating decay rates.

DOI: 10.1103/PhysRevB.73.165305 PACS number(s): 78.67.Hc, 31.15.Kb

I. INTRODUCTION

The small size and strong optical properties of self-assembled quantum dots (QDs) make them appealing candidates for optoelectronic devices.[1,2] When light is absorbed, photons create electron-hole (*eh*) pairs (excitons) that become confined in the quantum dot. Recent photoluminescence (PL) spectra have measured the recombination energy of electron-hole pairs with meV resolution.[3,4] Analysis of single dot PL spectra at different incident light intensities reveals that the exciton recombination energy is shifted by other "spectator" excitons and free charges in the dot.[3,4] For example, the recombination energy is redshifted a few meV by the presence of a spectator exciton.[3,4] Detailed understanding of the effect of spectators on recombination is important for nonlinear optical applications, such as quantum logic gates[5] or turnstiles.[6,7]

The rates of the PL processes determine the steady-state occupation of the dots for a given incident intensity.[4] Time-resolved photoluminescence measurements can track the electron-hole recombination rate in single self-assembled quantum dots.[4] Recent experiments give differing results about the decay rate of the biexciton relative to that of an isolated exciton in the same dot. Measurements on a single CdSe/ZnSe dot find a biexciton decay rate Γ_{XX} about equal to the exciton rate Γ_X,[8] while other experiments on similar sized CdSe/ZnSe QDs report a biexciton decay rate twice the exciton rate.[9] Similar measurements in InGaAs have found $\Gamma_{XX}/\Gamma_X \approx 1.5$,[4] $\Gamma_{XX}/\Gamma_X \approx 2$,[10,11] and even $\Gamma_{XX}/\Gamma_X \approx 0.33$.[12]

Theoretically, there are two limits to consider for recombination rates. In the strong confinement limit, the exciton and biexciton wave function is a simple product of the electron and hole single-particle wave functions in the dot. Coulomb interactions are assumed to only slightly perturb the wave function. In that case the recombination rates contain matrix elements of the single-particle wave functions, which are the same for excitons and biexcitons. Taking into account the number of allowed decay channels, the biexciton should decay at twice the exciton rate, $\Gamma_{XX}/\Gamma_X=2$. The other limit is the weak confinement limit, which applies when the exciton binding energy significantly exceeds the single-particle level spacing of the dot. In that limit, the exciton or biexciton is bulklike, bound together as a small composite particle. This exciton or biexciton unit is weakly confined in a dot much larger than the exciton or biexciton radius. In this case the dipole matrix element is dominated by the exciton or biexciton structure, which is independent of dot size. The composite particle has a coherent wave function that extends across the volume of the dot, leading to constructive addition of radiative matrix elements for exciton decay. Thus, in the weak confinement limit, the radiative decay rate of the exciton *increases* with dot size, until the dot diameter approaches the wavelength of the emitted light. For the biexciton, the exciton final state after recombination suppresses this constructive enhancement, significantly reducing the value of Γ_{XX}/Γ_X in the weak confining limit. In the intermediate regime, the exciton wave function generally cannot be separated, except for some special choice of the external potential, such as a harmonic confinement.[13] Still, the coherent extent of the many-particle wave function—the *coherence volume*[13]—leads to an increasing decay rate with increasing dot size and will play an important role in the interpretation of our results. In this paper we show that the radiative decay rates of typical self-assembled dots lie in the regime between strong and intermediate confinement.

Theoretical descriptions of single particle (electron or hole) states in quantum dots have improved greatly in the last ten years,[2,14–16] yet the description of exciton or multiexciton states is not as well developed. The energies of states with several electrons and holes are usually treated within first-order perturbation theory. Some spectral energies, such as the biexciton shift, require treatment of correlation with configuration interaction (CI) or quantum Monte Carlo (QMC) techniques.[17] The limited accuracy of approximate CI wave functions is known to affect the calculated energies.[17]

There have been a few attempts to calculate biexciton decay rates in quantum dots. Takagahara used a variational calculation to determine the decay rate of a biexciton in an infinite barrier spherical dot with dielectric effects.[18] More recently, Ungier[19] *et al.* have calculated the biexciton decay rate for zinc blende and wurtzite structures. Using CI expansions, Corni *et al.* have studied the size dependence of exciton and biexciton recombination rates in strain-induced dots.[20] These dots are formed in a near-surface InGaAs/GaAs quantum well by the stress field of an InP self-assembled island grown on the surface. These dots have much shallower confinement than self-assembled dots, are often much larger, and are well-approximated by truncated two-dimensional (2D) parabolic confinement. This puts the strain induced dots well into the weak confinement regime, contrary to the more common self-assembled dots that are subject of this paper. Recently, Narvaez *et al.* have performed CI calculations on InGaAs/GaAs self-assembled dots beyond the effective mass approximation using pseudopotentials.[21] These CI results must be viewed with some caution since decay rates are more sensitive than energies to errors in the wave function, as we will show in this paper.

In this paper we develop a Feynman path integral description of exciton and biexciton recombination rates. This technique can be easily applied to complicated dot geometries, does not depend on a finite basis set, and fully treats correlation. In Sec. II we derive a path-integral expression for the recombination rate. This expression is then evaluated using a real-space Monte Carlo technique that we introduce in Sec. III. In Sec. IV we apply our path integral technique to a model system and compare with full CI calculations. In Sec. V we apply both the path-integral technique and the CI expansion to realistic three-dimensional (3D) models of InGaAs/GaAs, CdSe/ZnSe, and InP/InGaP dots and compare to single-dot experiments. While our path-integral method is currently restricted to single-band effective mass approximation (EMA) models, the insights, trends, and even quantitative rates revealed in these make them quite useful, as we conclude in Sec. VI.

II. METHOD

Starting from a standard treatment of electron-hole radiative recombination in the effective mass approximation, we rewrite the square of the matrix element in the rate equation as a path-integral expression. In the path-integral formalism, we will show that the rate is proportional to the ratio of two path integrals: one with the standard thermal trace, and the other with a "radiating" configuration that pairs an electron and hole, as illustrated in Figs. 1(a) and 1(b).

A. Exciton recombination rate within the effective mass approximation

Our Hamiltonian is a commonly used effective mass model,

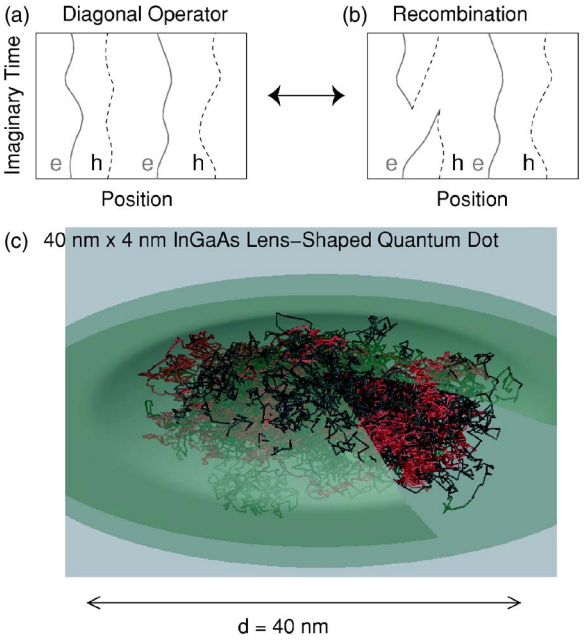

FIG. 1. (Color online) Illustration of our path-integral calculation of biexciton recombination rates in self-assembled quantum dots. We express the rate as a ratio of path integrals with (a) diagonal and (b) radiating constraints, see Eq. (6). We evaluate the path integrals using Monte Carlo integration on realistic three-dimensional models. A typical path contributing to the integrals for an InGaAs/GaAs dot is shown in (c). These paths sample the probability density, energy, rate, and other properties of the radiating states.

$$H = \sum_{N_h} \left(\frac{\mathbf{p}_h^2}{2m_h^*} + V_h(\mathbf{r}_h) \right) + \sum_{N_e} \left(\frac{\mathbf{p}_e^2}{2m_e^*} + V_e(\mathbf{r}_e) \right) + \frac{1}{2} \sum_{i \neq j} \frac{q_i q_j}{\epsilon r_{ij}}, \tag{1}$$

where V_e and V_h describe a lens-shaped confining potential and the hole effective masses m_h are anisotropic. In contrast to previous approaches to this problem, we do not construct single-particle or variational wave functions. Rather, we use Metropolis Monte Carlo to sample the recombination rate directly from a path-integral. The path-integral Monte Carlo (PIMC) method allows us to calculate the density matrix for the Hamiltonian, Eq. (1). As we describe below, this is an essentially exact solution without basis set problems or the difficulties of variational approaches. A snapshot of a typical path for an electron-hole pair in our simulation is shown in Fig. 1(c). A sum over all such paths is a complete quantum mechanical solution for the model, Eq. (1).

The rate of spontaneous decay of an exciton into a photon is the sum of the rates of all possible decay processes. For generality, we consider a state Φ_i^α with N electron-hole pairs decaying to a state Φ_f^α with $N-1$ pairs. The rate of spontaneous emission into a photon with polarization $\hat{\lambda}$, momentum $\hbar\mathbf{k}$, and energy $\hbar\omega$, in a medium with index of refraction n ($\approx\sqrt{\epsilon}$), is

$$\frac{d\Gamma^{\alpha}_{\mathbf{k}\hat{\lambda}}}{d\Omega} = \frac{n\omega e^2}{hc^3}|\langle\Phi^{\alpha}_f|\mathbf{j}_{\mathbf{k}\hat{\lambda}}\cdot\hat{\lambda}|\Phi^{\alpha}_i\rangle|^2, \tag{2}$$

which follows from Fermi's golden rule. Since the emitted photon has energy slightly less than the band gap (typically 1–3 eV), the photon wavelength is much greater than the dimensions of the self-assembled dot (typically 5–50 nm), so we take the $\mathbf{k}\to 0$ limit in the current operator, $\mathbf{j}_{\mathbf{k}\to 0,\hat{\lambda}}$. The usual approximation for the exciton decay rates in semiconductors is to use the envelope approximation, in which the single-particle wave functions are approximated as an envelope times a periodic Bloch function, $\phi(\mathbf{r})=\psi(\mathbf{r})u(\mathbf{r})$. Then the current operator splits into a delta function on the envelope and the current operator $\mathbf{j}=\mathbf{p}/m$ on the Bloch function. The momentum matrix element between the conduction band (CB) and valence band (VB) Bloch functions is given by the Kane parameter, $E_{\mathrm{P}}=2|\langle \mathrm{CB}|\mathbf{p}|\mathrm{VB}\rangle|^2/m$. Since all significant transitions occur in an energy range given by the Coulomb interaction (a few tens of meV), which is much smaller than the gap energy, we take the usual approximation $\hbar\omega\approx E_{\mathrm{gap}}$. Thus, within the envelope approximation, the recombination rate due to transition α is approximately

$$\Gamma^{\alpha} = \frac{2nE_{\mathrm{gap}}E_{\mathrm{P}}e^2}{3\hbar^2c^3m}|I^{\alpha}_N|^2, \tag{3}$$

where the point contact matrix element I is the overlap integral of the initial and final envelope functions,

$$I^{\alpha}_N = \int \psi^{\alpha *}_N(\mathbf{R}_N)\psi^{\alpha}_{N-1}(\mathbf{R}_{N-1})\,\delta^3(\mathbf{r}^e_N-\mathbf{r}^{\mathrm{h}}_N)d^{3N}\mathbf{R}_N. \tag{4}$$

B. Path integral expression for the rate

The determination of exciton and biexciton recombination rates using Eqs. (3) and (4) faces two difficulties. First, the initial and final states contain several interacting particles, for which correlation must be treated carefully. Second, the total rate is a sum over all possible transitions, $\Gamma=\Sigma_{\alpha}\Gamma^{\alpha}$. These difficulties may be treated explicitly for model systems (such as harmonic oscillators), but generally the direct determination of the matrix elements and rates in a wave function representation leads to approximations. For example, Takagahara's variational calculation[18] treats correlation very well for a single transition from a biexciton to the exciton ground state, but is limited to very symmetric, spherical QDs. On the other hand, Ungier[19] *et al.* treat material details in the bulk with much care (even beyond the envelope function above), but the correlation is only partially included, an approximation known to underestimate biexciton binding energies.[17] CI calculations can in principle solve the full many-particle Schrödinger equation for excitons and biexcitons for EMA models[20] and pseudopotentials,[21] but may be severely limited by the underlying basis set, as we will show.

We now derive a path-integral solution for the total recombination rate that will fully treat correlation, thermally distribute the initial states, and include all final states. To relate Eqs. (3) and (4) to a path integral, we begin by squaring the point contact matrix element,

$$|I^{\alpha}_N|^2 = \int\int \rho^{\alpha}_N(\mathbf{R}_N,\mathbf{R}'_N)\rho^{\alpha}_{N-1}(\mathbf{R}'_{N-1},\mathbf{R}_{N-1}) \times \delta(\mathbf{r}^e_N-\mathbf{r}^{\mathrm{h}}_N)\,\delta(\mathbf{r}^{e'}_N-\mathbf{r}^{\mathrm{h}'}_N)d\mathbf{R}_N d\mathbf{R}'_N, \tag{5}$$

where ρ^{α}_N and ρ^{α}_{N-1} are the density matrices of the initial and final states. As in Ref. 3, we assume that the carriers reach thermal equilibrium before the transition, and use the thermal density matrix of N electron-hole pairs, $\rho_N(\mathbf{R}_N,\mathbf{R}'_N;\beta)$. The final state can take on any value, so we sum over all final states, yielding $\rho_{N-1}(\mathbf{R}'_{N-1},\mathbf{R}_{N-1})=\delta^{3(N-1)}(\mathbf{R}_{N-1}-\mathbf{R}'_{N-1})$. After integrating out the $\mathbf{R}'_N$ coordinates in Eq. (5) with this delta function and using Eq. (3), we find the temperature-dependent radiative recombination rate,

$$\Gamma_N(\beta) = \frac{2nE_{\mathrm{gap}}E_{\mathrm{P}}e^2}{3\hbar^2c^3m}\langle|I_N|^2\rangle_{\beta}, \tag{6}$$

where

$$\langle|I_N|^2\rangle_{\beta} = Z_N^{-1}\int\int \rho_N(\mathbf{R}_N,\mathbf{R}'_N;\beta)\,\delta(\mathbf{R}'_{N-1}-\mathbf{R}_{N-1}) \times \delta(\mathbf{r}^e_N-\mathbf{r}^{\mathrm{h}}_N)\,\delta(\mathbf{r}^{e'}_N-\mathbf{r}^{\mathrm{h}'}_N)d\mathbf{R}_N d\mathbf{R}'_N. \tag{7}$$

In this equation $Z_N\equiv \mathrm{Tr}\,\rho_N$ is the partition function for N electron-hole pairs and is needed to normalize ρ_N in the integral.

The thermal density matrix in Eq. (6) may be represented as a real-space Feynman path integral,[22]

$$\rho(\mathbf{R}_N,\mathbf{R}'_N;\beta) = \int \mathcal{D}\mathbf{R}_N(t)\exp\left[-\frac{1}{\hbar}\int_0^{\beta} H dt\right], \tag{8}$$

where the ends of the paths are $\mathbf{R}_N(0)=\mathbf{R}'_N$ and $\mathbf{R}_N(\beta)=\mathbf{R}_N$. Thus the partition function Z_N and the recombination integral $\langle|I_N|^2\rangle_{\beta}$ can be represented by path integrals that differ only by constraints on the paths,

$$Z_N = \int_{\mathrm{diagonal}} \mathcal{D}\mathbf{R}_N(t)\exp\left[-\frac{1}{\hbar}\int_0^{\beta} H dt\right], \tag{9}$$

$$Z_N\langle|I_N|^2\rangle_{\beta} = \int_{\mathrm{radiating}} \mathcal{D}\mathbf{R}_N(t)\exp\left[-\frac{1}{\hbar}\int_0^{\beta} H dt\right]. \tag{10}$$

The diagonal constraint is the usual trace, $\mathbf{R}_N(0)=\mathbf{R}_N(\beta)$, illustrated in Fig. 1(a). The radiating constraint is a trace over the nonradiating pairs, $\mathbf{R}_{N-1}(0)=\mathbf{R}_{N-1}(\beta)$, and a pairing of the recombining particles, $\mathbf{r}^e_N=\mathbf{r}^{\mathrm{h}}_N$ and $\mathbf{r}^{e'}_N=\mathbf{r}^{\mathrm{h}'}_N$, as illustrated in Fig. 1(b). For the sake of clarity, the times $t=0$ and $t=\beta$ are plotted in the middle of the world-line diagrams of Fig. 1, as the paths are periodic in imaginary time.

It is insightful to consider how this path-integral formalism for the recombination rate, Eq. (6), relates to the strong and weak confinement limits. Consider the $t=0$ slice in imaginary time. In the diagonal boundary conditions, the path-integral samples the diagonal of the density matrix in the position basis. For a noninteracting exciton or biexciton, the electron and hole sample the probability density functions of the single-particle electron and hole ground states. In

the radiating boundary condition, the electron and hole are forced to coincide, but may sample two different points for $t=0_-$ and $t=0_+$. The effects approximately cancel out, giving $\langle|I_N|^2\rangle_\beta \sim 1$, appropriate for the strong confinement limit. With the attractive *eh* interaction in the weak confinement limit, the electron and hole pair together in an exciton. In the diagonal boundary conditions, the volume sampled by the electron and hole is the dot volume V_{dot} times the exciton volume $\sim a_X^3$. In the radiating boundary conditions, the volume sampled is V_{dot} for $t=0_-$ times another factor of V_{dot} for $t=0_+$. This gives $\langle|I_N|^2\rangle_\beta \sim V_{\mathrm{dot}}/a_X^3$, appropriate for the weak confinement limit with dot diameter much less than the wavelength of light.

Now consider a bound biexciton. One exciton has radiating boundary conditions and the other exciton has diagonal boundary conditions. For the strong confining case we see a similar cancellation of boundary condition effects as for the single exciton. Since we have contributions from pairing either the spin-up or spin-down electrons and holes, we see $\Gamma_{XX}/\Gamma_X \approx 2$. In the weak confining limit, the *eh* pair in the radiating boundary condition is bound to the other *eh* pair in the diagonal boundary condition, with a biexciton radius a_{XX}. This binding suppresses a factor of V_{dot} in the biexciton rate, leading to a reduced relative rate, $\Gamma_{XX}/\Gamma_X \sim 2a_{XX}^3/V_{\mathrm{dot}}$. While this ratio may drop below one for very large dots, most self-assembled dots are not much bigger than biexcitons, so we would not expect to see this limit except in extreme cases.

III. COMPUTATIONAL METHODOLOGY

The path integral expression for the recombination rate can be directly sampled with Monte Carlo integration, for two- or four-particle interacting quantum systems. We have implemented this as a computer simulation that allows for anisotropic masses and any three-dimensional confining potential we choose.

A. Path-integral Monte Carlo

With the use of Monte Carlo integration, the path-integral approach allows an essentially exact numerical solution to many quantum statistical problems.[23] Quantum Monte Carlo methods have been useful for problems related to this one, such as trion binding energies in quantum wells,[24] multiexciton energies in quantum dots,[17] and positron-electron annihilation rates,[25] as well as bulk phenomena, such as exciton-exciton scattering[26] and Bose condensation of excitons.[27]

To compute $\langle|I_N|^2\rangle_\beta$ we define a density matrix that contains both radiating *and* diagonal constraints

$$\tilde{\rho}(\mathbf{R}_N,\mathbf{R}'_N) = \rho_{\mathrm{rad}}(\mathbf{R}_N,\mathbf{R}'_N) + \rho_{\mathrm{diag}}(\mathbf{R}_N,\mathbf{R}'_N), \tag{11}$$

where

$$\rho_{\mathrm{rad}}(\mathbf{R}_N,\mathbf{R}'_N) = \rho_N(\mathbf{R}_N,\mathbf{R}'_N)\,\delta(\mathbf{R}_{N-1}-\mathbf{R}'_{N-1}) \times \delta(\mathbf{r}_N^e-\mathbf{r}_N^{\mathrm{h}})\,\delta(\mathbf{r}_N^{e'}-\mathbf{r}_N^{\mathrm{h}'}) \tag{12}$$

and

$$\rho_{\mathrm{diag}}(\mathbf{R}_N,\mathbf{R}'_N) = \rho_N(\mathbf{R}_N,\mathbf{R}'_N)\,\delta(\mathbf{R}_N-\mathbf{R}'_N). \tag{13}$$

Since the radiating and diagonal constraints form two disjoint subsets in configuration space we can write the probability of being in either state as

$$P(\text{radiating/diagonal state}) = \int \tilde{Z}^{-1}\rho_{\mathrm{rad/diag}}(\mathbf{R}_N,\mathbf{R}'_N)\,d\mathbf{R}_N\,d\mathbf{R}'_N, \tag{14}$$

where $\tilde{Z}=\int\tilde{\rho}(\mathbf{R}_N,\mathbf{R}'_N)\,d\mathbf{R}_N\,d\mathbf{R}'_N$. Combining Eqs. (7) and (14), we get an expression suitable for evaluation within PIMC:

$$\langle|I_N|^2\rangle_\beta = \frac{P(\text{radiating state})}{P(\text{diagonal state})}. \tag{15}$$

In our simulations we use a path-integral expansion of the density matrix ρ_N with a finite number of imaginary time slices. The configuration space of this expansion is $(\mathbf{R}_N^{(0)}=\mathbf{R}_N,\mathbf{R}_N^{(1)},\ldots,\mathbf{R}_N^{(m)}=\mathbf{R}'_N)$ where m is the number of time slices. We sample the probability distribution $\tilde{Z}^{-1}\tilde{\rho}$ using the Metropolis algorithm. Since the number of time slices m is of order 10^4 in a typical calculation, it is essential to use a multilevel Metropolis algorithm,[23] especially when changing the configuration from radiating to diagonal state and vice versa. The probability of being in either state can then be estimated from the relative frequencies x_{rad} and $x_{\mathrm{diag}}=1-x_{\mathrm{rad}}$ of radiating and diagonal path configurations in the Markov chain.

Finally, we arrive at $\langle|I_N|^2\rangle_\beta \approx x_{\mathrm{rad}}/x_{\mathrm{diag}}$, and from Eq. (6) we get the radiative recombination rate,

$$\Gamma_N(\beta) = \frac{2nE_{\mathrm{gap}}E_{\mathrm{P}}e^2}{3\hbar^2c^3m}\frac{x_{\mathrm{rad}}}{x_{\mathrm{diag}}}. \tag{16}$$

When calculating rates, we use the exciton energies from the simulation for E_{gap}.

Since the temperature $k_{\mathrm{B}}T$ in our simulations is small compared to the single-particle level spacing in the dot, we can assume that electrons and holes in the biexciton are in a singlet state, $S=0$. Therefore, the fermion sign problem does not occur in our calculations. (For a review on the origin of the sign problem, see, e.g., Ref. 28.) Instead of simulating an $S=0$ ensemble (symmetric wave function) for the electrons and holes in the biexciton, we sample an $S_z=0$ ensemble of distinguishable particles which includes both singlet and triplet states, but which has $S=0$ as the lowest eigenstate. As in this study we are only interested in ground state properties of excitons and biexcitons, the algorithm can be kept simple by treating the same-type particles as distinguishable. When studying temperature dependence, it is necessary to explicitly symmetrize the density matrix via permutations of same-type carriers,[23] since then the excited states become important.

B. Configuration interaction calculations

To demonstrate our method, we have also performed CI calculations on the same EMA models, Eq. (1). The single-particle states are calculated by finite-difference discretiza-

tion in a cylindrical cell with 30 nm height and 100 nm diameter, with grid spacing of 0.5 nm and 0.8 in the vertical and radial directions, respectively; Coulomb integrals are evaluated by successive over relaxation. This is the same approach used to calculate multiexciton states reported in Ref. 29.

For the simulation of excitons and biexcitons in self-assembled QDs, our CI expansion uses a $6s5p4d3f2g2h1i$ basis set, including 44 single-particle states. In contrast, the CI expansion by Corni *et al.* uses a $4s4p3d$ basis set (18 single-particle states) in the xy plane and only a single state for the z direction consisting of Gaussians centered on the dot. Contrary to the direct expansion of the many-particle wave function in our approach, Corni *et al.* use this basis set first to solve the restricted Hartree-Fock equation to obtain an optimized basis set for the CI expansion. Like our approach, the CI calculations by Narvaez *et al.* also use single-particle states from a noninteracting Hamiltonian to expand the many-body wave function. No basis set size is given in Ref. 21, but a previous paper by the same authors using an identical method used six electron and ten hole states (12 electron and 20 hole states including spin).[30]

IV. TESTS ON PARABOLIC DOT

To compare our methods, we first consider a model system consisting of two oppositely charged particles in a harmonic oscillator potential ("Hooke exciton"). The Hamiltonian then reads

$$H = \sum_{i=1}^{2} \left(\frac{\mathbf{p}_i^2}{2m_i} + \frac{m_i \omega^2}{2} \mathbf{r}_i^2 \right) - \frac{e^2}{\epsilon |\mathbf{r}_1 - \mathbf{r}_2|}. \tag{17}$$

Using center-of-mass and relative coordinates, the problem reduces to an ordinary differential equation (ODE) that can be integrated numerically with almost arbitrary exactness. We apply both the PIMC and CI techniques to this system. Within the path-integral calculations we use a temperature of $\beta = 10\mathrm{Ha}^{*-1}$, which is low enough to ensure that only the ground state contributes, and $m = 500$ time slices. The CI calculations use 54 single-particle states to expand the two-particle wave function.

Figure 2(a) shows the total and the binding energy of the two particles as a function of the harmonic confinement. Both CI and PIMC show very good agreement with the results from numerical integration of the ODE. However, for $|I_N|^2$ only PIMC shows good convergence whereas the CI results are in general too low, up to a factor of 2 in the weak confinement case. But even for strong confinement there is a considerable discrepancy, although the confinement energy significantly exceeds the exciton binding energy [see Fig. 2(b)]. In our calculations we have also found that the CI result for $|I_N|^2$ approaches the correct value rather slowly with increasing basis set size, thus leading to a false impression of convergence. If only the dependence of the result on the basis set is used as a measure of convergence, it is hard to decide whether a calculation has converged or not.

The true many-particle wave function for Coulombic interactions must have a coalescence cusp for $\mathbf{r}_1 = \mathbf{r}_2$,[31] but a CI expansion of the wave function in products of smooth single-particle basis functions cannot have a nonanalytic behavior. Convergence problems of CI associated with the failure to reproduce this cusp are, for example, solved by using correlated basis functions (e.g., Ref. 32). It is therefore not surprising that CI calculations give better results for energies than for the overlap matrix element: The energy is calculated using the wave function at every grid point, whereas for the decay rate mainly the cusp at $\mathbf{r}_1 = \mathbf{r}_2$ enters. That the overlap matrix element is more sensitive to errors in the wave function than the energy, also shows in the fact that even a Hartree-Fock calculation gets up to 95% of the exciton binding energy[17] but completely lacks the correlation cusp, leading to a decay rate that does not depend on the dot size.[20] Still, it is striking that the CI results are able to reproduce energies very accurately and yet completely fail to obtain the correct overlap matrix element. PIMC does not suffer from a finite basis set and can thus reproduce both energies and the overlap matrix element very accurately.

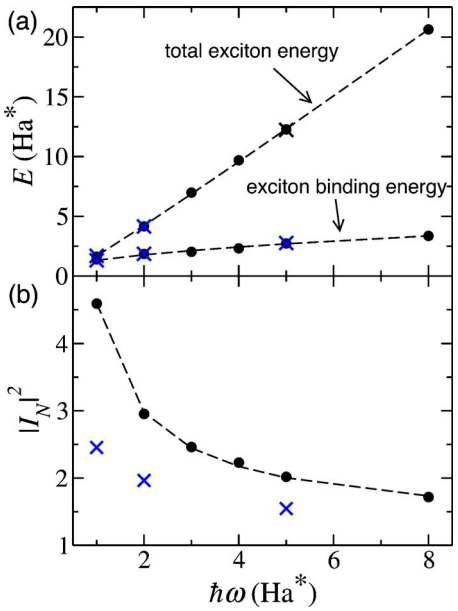

FIG. 2. (Color online) Comparison of results for Hooke exciton from PIMC and CI (expansion in 54 basis states): (a) total and binding energies and (b) $|I_N|^2$ from integration of ODE, from PIMC and CI (dashed line, circles, and ×'s). Energies are given in units of reduced Hartrees $\mathrm{Ha}^* = \mu e^4/\hbar^2\epsilon^2$, where μ is the reduced mass of the exciton. Error bars are of the order of symbol size.

V. RESULTS FOR SELF-ASSEMBLED DOTS

We have applied these techniques to common single-band effective mass models of quantum dots, summarized in Table I. We chose these materials and sizes because of availability of published experimental values. The dot geometry is a lens shape, with a height to diameter ratio of 1:10. The calculations include a wetting layer, modeled as a quantum well with thickness t_{WL} extending from the base of the dot. The dot potential consists of potential steps of finite height V_e (V_h) for electrons (holes) at the boundaries of the lens and the wetting layer. The three systems we have studied are:

TABLE I. Single-band effective mass parameters used in the calculations.

dot/barrier	$E_{\mathrm{gap}}^{\mathrm{barrier}}$ (eV)	ϵ	m_e	$m_h^{\parallel}$	$m_h^{\perp}$	ΔV_e (eV)	ΔV_h (eV)	t_{WL} (Å)	E_{P} (eV)
$In_{0.5}Ga_{0.5}As/GaAs$	1.519[a]	12.5[b]	0.067[b]	0.11[b]	0.38[b]	0.250[c]	0.200[c]	16, 0	25.7[b]
$InP/In_{0.5}Ga_{0.5}P$	1.920[d]	12.6[e]	0.079[e]	0.150[e]	0.600[e]	0.420[d]	0.070[d]	5	20.4[e]
CdSe/ZnSe	2.820[a]	9.3[f]	0.130[f]	0.380[g]	1.000[g]	0.735[h]	0.135[h]	5	17.5[g]

[a]Reference 33.
[b]We approximate the strained InGaAs material in the dot by just taking the bulk GaAs value (Ref. 33).
[c]Estimated from strain-modified band offsets plotted in Ref. 34.
[d]Estimated from empirical pseudopotential method (EPM)/valence force field(VFF) calculations (Nair, unpublished).
[e]Bulk InP value (Ref. 33).
[f]Bulk CdSe values (Ref. 33).
[g]Reference 35.
[h]CdSe/ZnSe band offsets chosen to match simulations in Ref. 36.

1. *InGaAs/GaAs*: This is the most studied material for optical properties of self-assembled dots, and we are comparing our results with four separate PL rate experiments. Some of these dots are grown as alloyed InGaAs material, while others are nominally pure InAs. Even for nominally pure dots, intermixing and annealing at high temperatures often leads to dots with significant Ga content. Based on reported growth conditions and PL energies, we have chosen to simulate dots composed of $In_{0.5}Ga_{0.5}As$. The dot diameters, from 10 nm to 60 nm, cover the size range for nearly all dots of this material reported in PL studies. We have included a 6 monolayer (ML), or 16 Å, $In_{0.5}Ga_{0.5}As$ wetting layer under the dot.[1] To show the influence of the wetting layer we also give results for $t_{\mathrm{WL}}=0$.

2. *InP/InGaP*: We have included a 2 ML, or 5 Å, InP wetting layer under the dot.

3. *CdSe/ZnSe*: We have included a 2 ML, or 5 Å, CdSe wetting layer under the dot.[37]

In this study, the effective masses are kept constant throughout the simulation region. We have made this approximation to keep the algorithm simple, but the simulation of a position-dependent mass is possible. Mathematically, the issue is the same as sampling random walks with a position-dependent diffusion constant. Similar quantum Monte Carlo techniques have been used to sample pseudo-Hamiltonians[38] containing terms equivalent to a position-dependent mass. Another issue is the effect of band nonparabolicity and band mixing. Band nonparabolicity can be included directly in the PIMC approach, as demonstrated in Ref. 39. Full multiband models are more complicated, and path-integral Monte Carlo for six- or eight-band $\mathbf{k}\cdot\mathbf{p}$ has not yet been realized. For simplicity in presentation, all our calculations are restricted to single-band, position-independent effective masses, and this approximation should be considered in the comparison to experiments.

While our path-integral formalism allows for a thermal distribution of initial states, we have chosen a low temperature ($T\approx 8$ K) so that we consider only emission from the ground state. We have discretized imaginary time in the path integral in steps of $\tau=1.3\times10^{-5}$ K^{-1}. The simulation time for one dot diameter was approximately 200 min for the exciton and 350 min for the biexciton on 10 Athlon MP 1600+ processors.

In Fig. 3 we present results of our path-integral calculations, along with our CI results and published experimental data points. In Fig. 3(b) we see that the absolute exciton decay rate Γ_X increases for large dots with increasing dot diameter due to the larger exciton coherence volume. As already expected from our model calculations, the CI results for the decay rate suffer from underconvergence, although the exciton energies from PIMC and CI agree very well. This is particularly evident in the decay rate for CdSe/ZnSe where the CI result begins to saturate for large dot sizes due to missing correlation, whereas the Monte Carlo result still increases uniformly with increasing dot diameter. A similar flattening of the decay ratio with increasing dot diameter can also be observed in the CI results of Corni *et al.*, possibly indicating missing correlation at larger dot sizes.[20] For small dots, we observe a minimum of the decay rate when the dot height h becomes comparable to the wetting layer thickness t_{WL}. The InGaAs/GaAs dots without wetting layer do not show this behavior. Note that in this case we only give results down to dot diameter $d=15$ nm, because the exciton becomes unbound for smaller dot sizes. The exciton decay rate in the InGaAs/GaAs material system is larger for $t_{\mathrm{WL}}=16$ Å than for $t_{\mathrm{WL}}=0$ Å since the effective dot size and thus the exciton coherence volume is larger for the dots including a wetting layer.

The relative decay rate Γ_{XX}/Γ_X of the biexciton, Fig. 3(a), varies from approximately 2 down to 1.5 for InGaAs/GaAs and InP/InGaP and even down to 1 for the CdSe/ZnSe material system. For large dots we observe a decrease of Γ_{XX}/Γ_X for increasing dot size, at small dot sizes there is a maximum of the relative biexciton decay rate corresponding to the minimum in the exciton decay rate. Again, the data for InGaAs/GaAs without wetting layer does not show an extremum for small dots but reaches $\Gamma_{XX}/\Gamma_X\approx 2$, corresponding to the strong confinement or noninteracting limit. As we explained above, CI underestimates decay rates. However, since it underestimates both exciton and biexciton decay rates, the relative ratio from CI is actually rather similar to the Monte Carlo result.

To gain more insight into the size dependence of the decay rates, it is useful to study the spatial extent of the exciton wave function in the dot. The decay rate is closely linked to the coherence volume and thus to the volume that is filled by

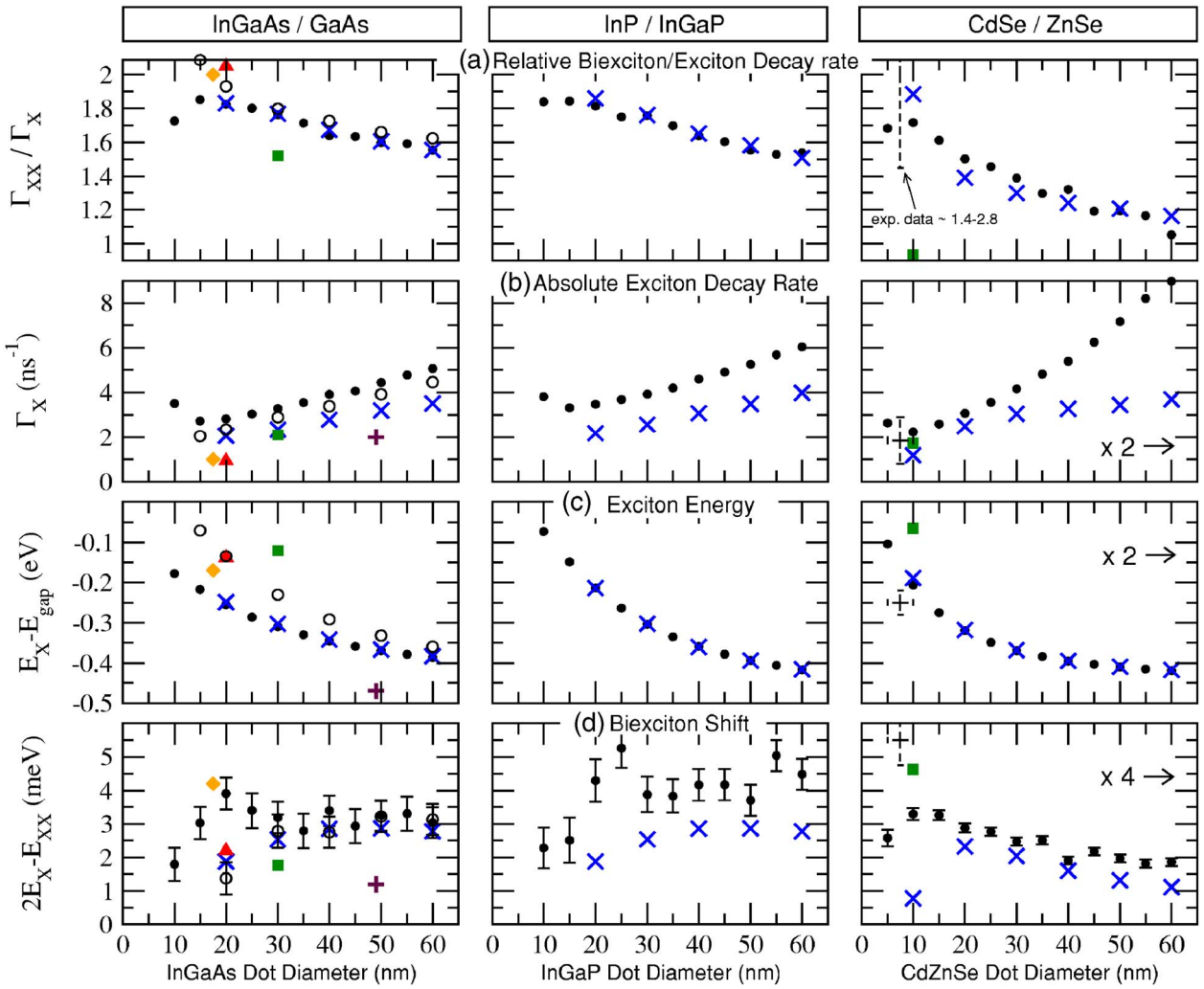

FIG. 3. (Color online) Our results of path-integral calculations for InGaAs/GaAs, InP/InGaP, and CdSe/ZnSe lens-shaped dots of different diameters, with height/diameter=0.1. Rows of panels present (a) the relative decay rate of biexciton to exciton, (b) the absolute decay rate of exciton, (c) the exciton energy, at which the exciton luminescence peak would be observed, and (d) the energy shift of the biexciton luminescence peak. Solid circles are path integral results for $t_{WL}>0$, open circles for $t_{WL}=0$. Error bars are only given if the error exceeds the symbol size. We compare to our configuration interaction calculations for $t_{WL}>0$ (×'s), which miss some of the correlation. We also show experimental data for InGaAs/GaAs (△'s are data from Ref. 10, where we have assumed $d=20$ and used their measured X^* and XX^* data points; □'s are data from Ref. 4, ◇'s are from Ref. 11, +'s are from Ref. 12) and for CdSe/ZnSe (□'s are data from Ref. 8, the range of data from Ref. 9 is indicated by dashed crosses).

the exciton wave function. In Fig. 4 we present the size dependence of the exciton radius a_X and the standard deviation of the exciton center-of-mass (com) coordinate $\Delta r_{com} = \sqrt{\langle \mathbf{r}_{com}^2 \rangle - \langle \mathbf{r}_{com} \rangle^2}$ for the InGaAs/GaAs and CdSe/ZnSe material systems. The results for InP/InGaP quantum dots are similar to those for InGaAs/GaAs, just as in Fig. 3.

For small dot sizes we find a minimum of both a_X and Δr_{com} corresponding to the minimum in the decay rate. As the dot height becomes comparable to the wetting layer thickness, the exciton center of mass moves into the wetting layer and the wave function extends further into the quantum well underneath the dot. A dot height less than t_{WL} thus corresponds to an effectively larger dot size. The increased coherence volume leads to an increase in the decay ratio Γ_X and a decrease of the relative biexciton ratio Γ_{XX}/Γ_X. In the limit of zero dot size, we would be in the quantum well situation; however, the dipole approximation leading to Eq. (3) does not hold for an extended quantum well state.[13] In the case of the QD without wetting layer, the coherence volume decreases monotonically until the exciton becomes unbound, thus we do not observe an extremum in the decay rates.

In the case of larger dot sizes we observe different behavior for InGaAs/GaAs and CdSe/ZnSe: In the case of InGaAs/GaAs, $\Delta r_{com} < a_X$ for all studied diameters and the exciton radius a_X does not show saturation towards the bulk value. With respect to these properties of the wave function, the dots are in the strong confinement limit, whereas the decay rate shows signatures of strong to intermediate confinement: The relative biexciton ratio can be tuned over a relatively large range—from 2 to 1.5—by changing the dot geometry, an effect entirely due to electronic correlation.

For CdSe/ZnSe we find a crossover to $\Delta r_{com} > a_X$ with increasing dot diameter. This corresponds to the weak confinement limit—an exciton "bouncing" around in the dot—

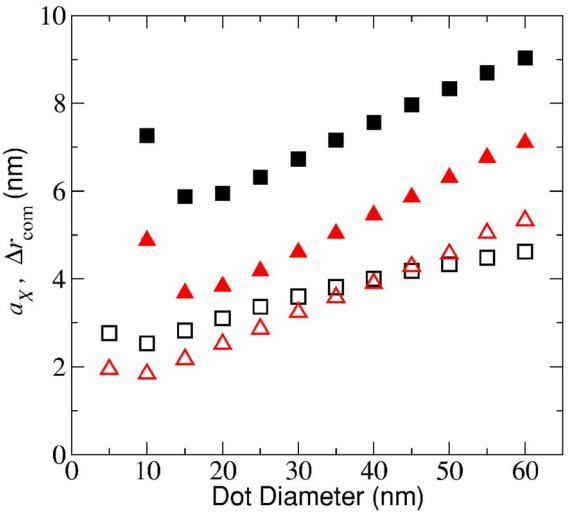

FIG. 4. (Color online) Exciton radius a_X (□'s) and exciton center of mass fluctuations Δr_{com} (△'s) for InGaAs/GaAs dots with a 6 ML wetting layer (full symbols) and for CdSe/ZnSe dots (open symbols).

and thus we observe relative biexciton ratios down to 1. However, reported photoluminescence measurements on this type of QDs are usually carried out on dots with a diameter d around 10 nm, so that the relevant experimental data for CdSe/ZnSe also lie in the strong to intermediate confinement regime.

When comparing to experiment, we notice that for some of the reported data our calculated exciton energies are much smaller than the experimental values. In these cases (Refs. 4 and 8) the growth conditions enhanced alloying. Our parameters for the band offsets do not seem to describe these shallow dots very well. However, since we use an abrupt potential step for the QD boundaries, the step height should not influence our calculated decay rates significantly, as long as the exciton is still bound. The step height just determines the exponential decay length of the wave function into the barrier, so its influence on the wave function inside the dot is only indirect. Comparison of our calculated results with these experiments is thus still valid.

In comparing to the work of Thompson *et al.*,[10] we found it was necessary to reidentify their reported exciton spectra line as a charged exciton. Our concerns were their reported negative (blue-shifted) biexciton binding energy and their ratio $\Gamma_{XX}/\Gamma_X \approx 2.3$. Their spectra are very similar to spectra reported by Lomascolo *et al.*, which are dominated by charged exciton,[40] only with the exciton/charged exciton labels switched. Since Thompson *et al.* called their identification of the charged and neutral exciton tentative, and did not offer any alternative explanation for the unusual energy shift and relative decay rate of their supposed neutral exciton/biexciton pair, we chose to compare to the data they had attributed to the charged exciton and charged biexciton. These states have $\Gamma_{XX}/\Gamma_X \approx 2.06$ and a biexciton binding energy of +2 meV. This identification makes little difference in our comparison of decay rates, but does give us much better agreement for the positive biexciton binding energy and is consistent with the relative biexciton decay rate in the strong-confinement limit. Thompson *et al.* do not give any value for the dot size in their experiment, but claim that their dots are smaller than those of other photoluminescence experiments. We chose to attribute their data a dot diameter of 20 nm, based on our energy calculations for the InGaAs/GaAs dot without wetting layer. In the absence of further information about the wetting layer thickness in the experiment, this seems reasonable since the nominal InAs coverage in this experiment is only 1.7 ML. Accordingly, we will always compare the experimental data from Thompson *et al.* as well as the data from Ulrich *et al.*[11] (experimental wetting layer thickness 1 ML) with the results of our calculation with $t_{WL}=0$ ML.

Our PIMC results for the exciton decay rate in InGaAs/GaAs agree with experiment within about a factor of 2, but seem to systematically overestimate the decay rate. This could be due to our simplified model of an ideal dot. The agreement with experiment could, for example, be improved by including the effects of alloying in the dot potential. Disorder introduced by alloying leads to stronger localization of the particles in the dot,[41] thus reducing the coherence volume and the electron-hole overlap. Another possiblity for improving the path-integral results would be to use a dot potential from strain calculations,[34] since strain might also lead to an increased electron-hole separation.[42] The inclusion of such single-particle potentials in PIMC is perfectly feasible and does not introduce any additional computational cost. Even in the strong confinement or noninteracting limit $|I_N|^2 \approx 1$, so $\Gamma_X \gtrapprox 2\ \mathrm{ns}^{-1}$ using the parameters from Table I. Thus the low decay rate from Refs. 10 and 11 cannot be explained in our model, hinting at the need of a more detailed dot potential. However, for the study of the size dependence of the decay rates a model potential is perfectly valid and yields results that are easier to interpret.

The Monte Carlo calculations can reproduce the range of observed relative biexciton ratios from 2 to 1.5. The data from Refs. 10 and 11 are described very well by the QD without wetting layer, whereas the data from Ref. 4 seem to be best reproduced by a QD with wetting layer, although we have to assume a somewhat larger effective dot size. The calculated biexciton binding energies are also close to the experimental values. The extremely low relative biexciton decay rate from Ref. 12, $\Gamma_{XX}/\Gamma_X=0.33$, however, cannot be explained at all in our model. In the original paper, the low biexciton decay rate was attributed to weak confinement effects, but from our calculations we can conclude that InGaAs/GaAs QDs with diameters around 50 nm are still far from the weak confinement regime.

We are not aware of any studies on the exciton and biexciton dynamics in single InP/InGaP QDs, but our calculations are within the reported exciton lifetime range of 100–500 ps for QD ensembles with dot diameters between 20 nm and 40 nm.[43]

When comparing to the experimental data on single CdSe/ZnSe dots by Patton *et al.*,[9] we chose to only give the range of the reported data. The variation of exciton energies in Patton *et al.* is attributed to different localization potentials, i.e., different Cd concentration, and not to different dot sizes. The dot diameter for their samples is reported to be between 5 nm and 10 nm.[44] The CdSe/ZnSe exciton decay rates calculated by PIMC agree very well with the reported

experimental data. However, we completely fail to reproduce the relative biexciton ratio $\Gamma_{XX}/\Gamma_X \approx 1$ from Bacher *et al.*[8] Such a low biexciton decay rate is only to be expected for very large dots in our simulation. The experiments by Patton *et al.* on very similar sized QDs in contrast yielded a relative biexciton ratio $\Gamma_{XX}/\Gamma_X \approx 2$ with a rather large experimental spread ($\Gamma_{XX}/\Gamma_X \approx 1.4-2.8$). We expect CdSe/ZnSe QDs of about 10 nm to be towards the strong confinement limit, consistent with the experiment by Patton *et al.* Therefore we presume that more knowledge about the dot potential would be needed to explain the results of Bacher *et al.*; a simple box model, as suggested in Ref. 8, is certainly not enough. The fact that the exciton energies from Ref. 9 are well explained by our model, whereas the rather shallow dots from Ref. 8 are not, supports this presumption. It should also be noted that the QDs of Ref. 45 were grown under conditions similar to those of Bacher *et al.* They show recombination energies and exciton lifetimes comparable to the results of Bacher *et al.*, but much shorter biexciton lifetimes. Since no estimate of the dot size was given, we cannot directly compare to our calculations, but the reported ratio of $\Gamma_{XX}/\Gamma_X \approx 1.4$ agrees well with the ratios expected from our calculation.

We cannot compare our hitherto obtained rates with the calculations of Corni *et al.* on the size dependence of the exciton and biexciton decay rates because of the different dot potentials. However, if we apply our technique to the truncated parabola potentials used in their study, we obtain exciton decay rates that are for small dots around 50%, and for large dots even up to two times larger than the results of Ref. 20. Given that even our CI expansion, using a large basis set of 44 single particle states, yields absolute rates that are too low, it is not surprising that the much smaller basis set of Corni *et al.* also fails to calculate absolute rates. Yet, the CI calculations show the right trends—increasing decay rate and decreasing Γ_{XX}/Γ_X with increasing dot size—compatible with our results. Also, the relative biexciton decay rate from PIMC is very similar to the one obtained by Corni *et al.*

Narvaez *et al.* have performed CI calculations on the height dependence of recombination rates in lens-shaped $In_{0.6}Ga_{0.4}As/GaAs$ quantum dots with a fixed diameter (25.2 nm), using atomic pseudopotentials and a realistic model for alloying. Their calculated decay rates lie in the range of $0.4-0.5\ ns^{-1}$, a factor of 4 lower than our results, but also a factor of 2 lower than experimental values.[10,11] Their reported relative biexciton decay ratio $\Gamma_{XX}/\Gamma_X=4$ is a factor of 2 larger than what is expected for strong confinement and is to our knowledge not observed in experiment. Path-integral techniques cannot be adapted to using pseudopotentials easily, and thus we cannot directly compare results. Still, from our experience with the calculation of rates from CI, we are somewhat concerned with the absolute value of the rates. The reported basis set size in Ref. 30 is much smaller than the one used in this study. For example, their minimum of the exciton lifetime (corresponding to a maximum in the decay rate) at a dot height of 65 Å could possibly be a sign of missed correlation at larger dot sizes: From our calculations we would expect the decay rate to grow monotonically with dot volume. The decrease of the exciton lifetime found at smaller dot heights, however, is compatible with our findings.

VI. CONCLUSION

We have developed a path-integral Monte Carlo approach for studying exciton and biexciton recombination rates in self-assembled quantum dots. This technique allows us to study general 3D potentials for a wide variety of single-band EMA models. Our calculations indicate that self-assembled dots are in the strong to intermediate confinement regime, where Coulomb correlation effects are becoming important. In particular, for large dots we see a clear monotonic rise in recombination rate versus diameter, and a decrease in the relative biexciton decay rate, Γ_{XX}/Γ_X. From our calculations we can state that relative decay rates $\Gamma_{XX}/\Gamma_X \approx 1.5-2$ are expected for typical photoluminescence experiments, an effect due entirely to correlation. We have seen that quantum dots of the size used in PL experiments tend towards the strong confinement regime. Thus, the low relative biexciton decay rates $\Gamma_{XX}/\Gamma_X \leqslant 1$ from some experiments,[8,12] that were attributed to weak confinement, cannot be explained by weak confinement effects. It should be noted that in single-dot experiments rather large dot-to-dot fluctuations have been reported.[9] Given the spread of experimental data, our calculations compare rather favorably against experiment.

We have further shown that CI expansions using uncorrelated single-particle basis sets have severe shortcomings in calculating decay rates. Rather surprisingly, we have found that CI expansion in a large basis set of 44 states underestimate decay rates by far, even for dot sizes comparable to the exciton Bohr radius and although the calculated energies were well-converged. Yet, due to a cancellation of errors, the relative biexciton decay rate calculated by CI was found to be similar to the path-integral result. Also, trends were in general reproduced correctly by CI. CI has some advantages over PIMC, such as being able to use an atomistic description of the quantum dot. However, absolute decay rates from CI must be regarded with caution.

In conclusion, we have developed a microscopic path-integral technique for calculating exciton and biexciton decay rates, that fully treats quantum correlation in realistic models. We can apply this to arbitrary geometries within single-band EMA models. Our calculations on lens-shaped self-assembled dots indicate that these commonly studied structures are in the regime between strong and intermediate confinement. The formalism has a built-in thermal distribution of carriers that we have not yet exploited. Another area for future research is an extension of this technique to semiconductors with indirect band gaps, such as Si/Ge.

ACKNOWLEDGMENTS

M.W. would like to thank J. Kainz and M. Schütz for useful discussions and acknowledges financial support from DFG within GRK 638. Work by J.S. was supported by NSF Grant No. DMR-0239819.

*Electronic address: Michael.Wimmer@physik.uni-regensburg.de
†Electronic address: john.shumway@asu.edu

[1] A. Wojs, P. Hawrylak, S. Fafard, and L. Jacak, Phys. Rev. B **54**, 5604 (1996).
[2] D. Bimberg, M. Grundman, and N. N. Ledentsov, *Quantum Dot Heterostructures* (John Wiley & Sons, New York, 1999).
[3] E. Dekel, D. Gershoni, E. Ehrenfreund, J. M. Garcia, and P. M. Petroff, Phys. Rev. B **61**, 11009 (2000).
[4] C. Santori, G. S. Solomon, M. Pelton, and Y. Yamamoto, Phys. Rev. B **65**, 073310(R) (2002).
[5] X. Li, Y. Wu, D. Steel, D. Gammon, T. H. Stievater, D. S. Katzer, D. Park, C. Piermarocchi, and L. J. Sham, Science **301**, 809 (2003).
[6] J. Kim, O. Benson, H. Kan, and Y. Yamamoto, Nature **397**, 500 (1999).
[7] A. Zrenner, E. Beham, S. Stufler, F. Findeis, M. Bichler, and G. Abstreiter, Nature **418**, 612 (2002).
[8] G. Bacher, R. Weigand, J. Seufert, V. D. Kulakovskii, N. A. Gippius, A. Forchel, K. Leonardi, and D. Hommel, Phys. Rev. Lett. **83**, 4417 (1999).
[9] B. Patton, W. Langbein, and U. Woggon, Phys. Rev. B **68**, 125316 (2003).
[10] R. M. Thompson, R. M. Stevenson, A. J. Shields, I. Farrer, C. J. Lobo, D. A. Ritchie, M. L. Leadbeater, and M. Pepper, Phys. Rev. B **64**, 201302(R) (2001).
[11] S. M. Ulrich, M. Benyoucef, P. Michler, N. Baer, P. Gartner, F. Jahnke, M. Schwab, H. Kurtze, M. Bayer, S. Fafard, Z. Wasilewski, and A. Forchel, Phys. Rev. B **71**, 235328 (2005).
[12] S. Kono, A. Kirihara, A. Tomita, K. Nakamura, J. Fujikata, K. Ohashi, H. Saito, and K. Nishi, Phys. Rev. B **72**, 155307 (2005).
[13] M. Sugawara, Phys. Rev. B **51**, 10743 (1995).
[14] A. J. Williamson and A. Zunger, Phys. Rev. B **59**, 15819 (1999).
[15] R. Heitz, O. Stier, I. Mukhametzhanov, A. Madhukar, and D. Bimberg, Phys. Rev. B **62**, 11017 (2000).
[16] R. Santoprete, B. Koiller, R. B. Capaz, P. Kratzer, Q. K. K. Liu, and M. Scheffler, Phys. Rev. B **68**, 235311 (2003).
[17] J. Shumway, A. Franceschetti, and A. Zunger, Phys. Rev. B **63**, 155316 (2001).
[18] T. Takagahara, Phys. Rev. B **39**, 10206 (1989).
[19] W. Ungier, Solid State Commun. **110**, 639 (1999).
[20] S. Corni, M. Braskén, M. Lindberg, J. Olsen, and D. Sundholm, Phys. Rev. B **67**, 045313 (2003).
[21] G. A. Narvaez, G. Bester, and A. Zunger, Phys. Rev. B **72**, 245318 (2005).
[22] R. P. Feynman, *Statistical Mechanics* (Addison-Wesley, Reading, MA, 1972).
[23] D. M. Ceperley, Rev. Mod. Phys. **67**, 279 (1995).
[24] A. S. Bracker, E. A. Stinaff, D. Gammon, M. E. Ware, J. G. Tischler, D. Park, D. Gershoni, A. V. Filinov, M. Bonitz, F. Peeters, and C. Riva, Phys. Rev. B **72**, 035332 (2005); A. V. Filinov, C. Riva, F. M. Peeters, Y. E. Lozovik, and M. Bonitz, *ibid.* **70**, 035323 (2004).
[25] S. Chiesa, M. Mella, and G. Morosi, Phys. Rev. A **69**, 022701 (2004).
[26] J. Shumway and D. M. Ceperley, Phys. Rev. B **63**, 165209 (2001); J. Shumway, Physica E (to be published).
[27] J. Shumway and D. M. Ceperley, J. Phys. IV **10**, Pr5 (2000).
[28] K. E. Schmidt and M. H. Kalos, in *Applications of the Monte Carlo Method in Statistical Physics*, edited by K. Binder (Springer-Verlag, Berlin, 1987).
[29] S. V. Nair and Y. Masumoto, Phys. Status Solidi B **224**, 739 (2000).
[30] G. A. Narvaez, G. Bester, and A. Zunger, Phys. Rev. B **72**, 041307(R) (2005).
[31] T. Kato, Commun. Pure Appl. Math. **10**, 151 (1957).
[32] W. Kutzelnigg and W. Klopper, J. Chem. Phys. **94**, 1985 (1991); V. Termath, W. Klopper, and W. Kutzelnigg, *ibid.* **94**, 2002 (1991); W. Klopper and W. Kutzelnigg, *ibid.* **94**, 2020 (1991).
[33] *Landolt-Börnstein: Numerical Data and Function Relationships in Science and Technology, Group III*, edited by O. Madelung, Vol. 17a (Springer-Verlag, Berlin, 1982).
[34] J. Shumway, A. J. Williamson, A. Zunger, A. Passaseo, M. DeGiorgi, R. Cingolani, M. Catalano, and P. Crozier, Phys. Rev. B **64**, 125302 (2001).
[35] A. I. Ekimov, F. Hache, M. C. Schanne-Klein, D. Ricard, C. Flytzanis, I. A. Kudryavtsev, T. V. Yazeva, A. V. Rodina, and A. L. Efros, J. Opt. Soc. Am. B **10**, 100 (1992).
[36] J. Puls, M. Rabe, H.-J. Wünsche, and F. Henneberger, Phys. Rev. B **60**, R16303 (1999).
[37] S. Lee, I. Daruka, C. S. Kim, A.-L. Barabási, J. L. Merz, and J. K. Furdyna, Phys. Rev. Lett. **81**, 3479 (1998).
[38] G. B. Bachelet, D. M. Ceperley, and M. G. B. Chiocchetti, Phys. Rev. Lett. **62**, 2088 (1989).
[39] J. Shumway, J. Phys.: Condens. Matter **17**, 2563 (2005).
[40] M. Lomascolo, A. Vergine, T. K. Johal, R. Rinaldi, A. Passaseo, R. Cingolani, S. Patanè, M. Labardi, M. Allegrini, F. Troiani, and E. Molinari, Phys. Rev. B **66**, 041302(R) (2002).
[41] G. Klimeck, F. Oyafuso, T. B. Boykin, R. C. Bowen, and P. von Allmen, Comput. Model. Eng. Sci. **3**, 601 (2002).
[42] S. Lee, J. C. Kim, H. Rho, C. S. Kim, L. M. Smith, H. E. Jackson, J. K. Furdyna, and M. Dobrowolska, Phys. Rev. B **61**, R2405 (2000).
[43] F. Hatami, W. T. Masselink, L. Schrottke, J. W. Tomm, V. Talalaev, C. Kristukat, and A. R. Goni, Phys. Rev. B **67**, 085306 (2003); F. Hatami, U. Müller, H. Kissel, K. Braune, R.-P. Blum, S. Rogaschewski, H. Niehus, H. Kirme, W. Neumann, M. Schmidbauer, R. Köhler, and W. T. Masselink, J. Cryst. Growth **216**, 26 (2000).
[44] F. Gindele, K. Hild, W. Langbein, and U. Woggon, Phys. Rev. B **60**, R2157 (1999).
[45] S. M. Ulrich, S. Strauf, P. Michler, G. Bacher, and A. Forchel, Appl. Phys. Lett. **83**, 1848 (2003).